Bioactive Materials 6 (2021) 3976–3986

Contents lists available at ScienceDirect

Bioactive Materials

journal homepage: www.sciencedirect.com/journal/bioactive-materials

Marginal sealing around integral bilayer scaffolds for repairing osteochondral defects based on photocurable silk hydrogels

Xiaolin Wu [1], Mingliang Zhou [1], Fei Jiang, Shi Yin, Sihan Lin, Guangzheng Yang, Yuezhi Lu, Wenjie Zhang [**], Xinquan Jiang [*]

Department of Prosthodontics, Shanghai Engineering Research Center of Advanced Dental Technology and Materials, Shanghai Key Laboratory of Stomatology, Shanghai Research Institute of Stomatology, National Clinical Research Center for Oral Diseases, Shanghai Ninth People's Hospital, College of Stomatology, Shanghai Jiao Tong University School of Medicine, No. 639 Zhizaoju Road, Shanghai, 200011, China

ARTICLE INFO

Keywords:
Integral bilayer scaffold
Photocurable Sil-MA hydrogel
Marginal sealing
Lateral integration
Osteochondral regeneration

ABSTRACT

Osteochondral repair remains a major challenge in current clinical practice despite significant advances in tissue engineering. In particular, the lateral integration of neocartilage into surrounding native cartilage is a difficult and inadequately addressed problem that determines the success of tissue repair. Here, a novel design of an integral bilayer scaffold combined with a photocurable silk sealant for osteochondral repair is reported. First, we fabricated a bilayer silk scaffold with a cartilage layer resembling native cartilage in surface morphology and mechanical strength and a BMP-2-loaded porous subchondral bone layer that facilitated the osteogenic differentiation of BMSCs. Second, a TGF-β3-loaded methacrylated silk fibroin sealant (Sil-MA) exhibiting biocompatibility and good adhesive properties was developed and confirmed to promote chondrocyte migration and differentiation. Importantly, this TGF-β3-loaded Sil-MA hydrogel provided a bridge between the cartilage layer of the scaffold and the surrounding cartilage and then guided new cartilage to grow towards and replace the degraded cartilage layer from the surrounding native cartilage in the early stage of knee repair. Thus, osteochondral regeneration and superior lateral integration were achieved in vivo by using this composite. These results demonstrate that the new approach of marginal sealing around the cartilage layer of bilayer scaffolds with Sil-MA hydrogel has tremendous potential for clinical use in osteochondral regeneration.

1. Introduction

Osteochondral regeneration has always been a major challenge due to the structure and properties of the osteochondral unit. As an integrated and functional whole, the osteochondral unit is anisotropic, with spatially varying compositional, structural and functional properties [1]. Bone tissue exhibits innate repair capability and the ability to regenerate in the presence of multiple cell types and the vasculature. Unlike bone regeneration, cartilage regeneration remains a difficult problem [2]. Articular cartilage, a translucent elastic tissue without blood vessels, lymphatic vessels or neural tubes, possesses limited innate self-healing ability [3]. Therefore, it is of great societal and academic significance to construct a high-performance cartilage repair scaffold and further orchestrate a bifunctional scaffold that guides cartilage and subchondral bone regeneration simultaneously to reconstruct full-thickness osteochondral defects.

Scaffold-based techniques have been widely used in osteochondral engineering since scaffolds can provide 3D microenvironments for endogenous or exogenous cells to augment cell adhesion, proliferation, migration, differentiation and mechanical support for newly formed tissues [4]. Recently, bilayer and multilayer scaffolds designed to mimic the anisotropic functional and structural characteristics of cartilage and bone tissue have achieved desired outcomes and attracted great attention [5–7]. However, the stable scaffold fixation and further tissue integration are often ignored. Integration is critical to the success of osteochondral regeneration because it provides stable biologic fixation, load distribution, and the appropriate mechanotransduction necessary for homeostasis [8,9]. After implantation at the defect site,

Peer review under responsibility of KeAi Communications Co., Ltd.
* Corresponding author.
** Corresponding author.
E-mail addresses: zhangwenjie586@126.com (W. Zhang), xinquanj@aliyun.com (X. Jiang).
[1] These authors contributed equally to this work.

https://doi.org/10.1016/j.bioactmat.2021.04.005
Received 19 February 2021; Received in revised form 21 March 2021; Accepted 5 April 2021

osseointegration to the scaffold readily occurs due to bone's high metabolism and cell content, including stem cells [10]. Because of the scaffold's intricate stratified structure, the vertical integration of cartilage to the underlying bone occurs to a considerable extent [11,12]. Nevertheless, the lateral integration of neocartilage to adjacent cartilage is a difficult problem that urgently needs to be solved [2].

Lateral integration is exceedingly difficult to achieve for the following reasons: 1) cartilage displays low metabolism and contains dense, anti-adhesive extracellular matrix (ECM) [13]. For example, proteins transcribed from the proteoglycan 4 (PRG4) gene, contributors to cartilage's low friction, and glycosaminoglycans (GAGs) have been shown to directly inhibit cell adhesion [14]; 2) the surgical preparation of defects results in cell death at the defect margins, further reducing integration potential [15]; and 3) upon loading, mismatches between the biomechanical properties of the implanted scaffolds and native cartilage tissue result in stress concentration, diminishing integration and damaging the surrounding tissue [8,16]. Hence, effective strategies to enhance lateral integration are reported rarely, if ever. To date, strategies to enhance lateral integration include antiapoptotic agents that mitigate cell death at the defect edge [15], matrix-degrading enzymes that decrease ECM antiadhesive properties [13], and, more recently, scaffold functionalization that enables direct bonding to adjacent cartilage [17]. However, all these studies focused on in vitro or subcutaneous implantation in nude mice without further validation of the effect on osteochondral repair in large animals. In addition, cartilage-cartilage integration in the mosaicplasty method was evaluated, but the integration of scaffold-guided neocartilage and the surrounding native cartilage in the tissue-engineering approach was not. Therefore, it is of vital importance to develop rehabilitation protocols that enhance lateral integration.

Silk fibroin (SF) is a natural fibrous polymer that has been applied for osteochondral engineering due to its biocompatibility, biodegradability, high tensile strength, and excellent biological characteristics [18–20]. Nonetheless, traditional silk scaffolds focus mainly on the porous structure of the cartilage layer, which is incompatible with the native cartilage structure and disadvantageous for cartilage formation [21–24]. In addition, bilayer or trilayer silk scaffolds are often combined with β-tricalcium phosphate (β-TCP) or ceramics as a subchondral bone layer to obtain high mechanical strength, which results in poor interface strength between the cartilage layer (silk) and the subchondral bone layer (β-TCP or ceramics) [18,25]. Therefore, an integral stratified silk scaffold designed to mimic osteochondral tissue is urgently needed. In addition, Park et al. recently designed and fabricated a silk-modified hydrogel with the addition of methacrylate groups to amine residues and subsequently realized cartilage tissue formation in the rabbit trachea via a chondrocyte-laden Sil-MA hydrogel [26]. However, cartilage tissue in joints needs to bear a load, which requires a high-strength scaffold for regeneration. Inspired by the application of medical glue or adhesive, we proposed this hydrogel as a marginal sealant to enhance lateral integration by utilizing its adhesive property [27,28].

In this study, we proposed an all-silk-derived composite consisting of integral bilayer scaffolds and marginal sealants for rapid and effective

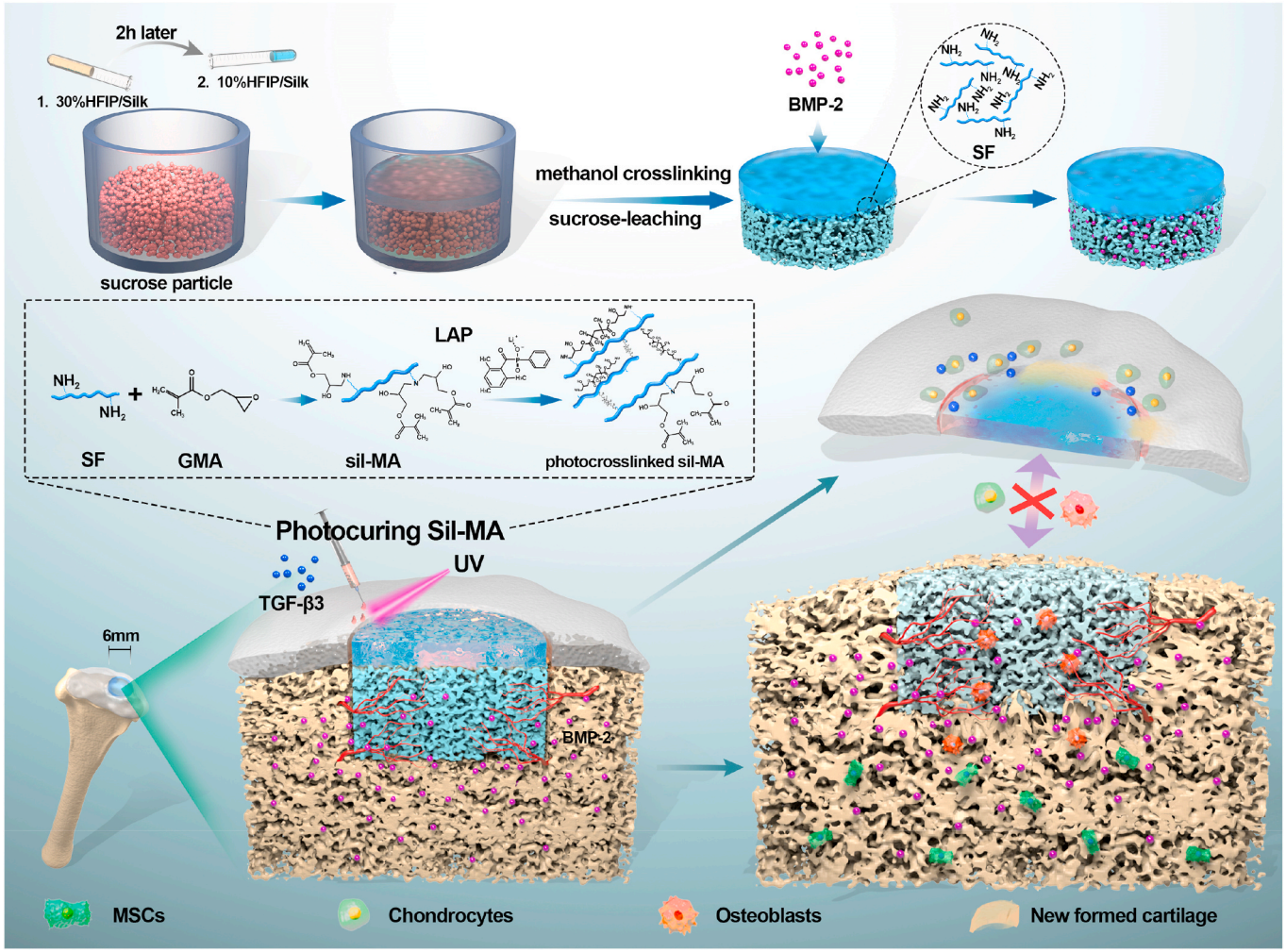

Fig. 1. Schematic illustration of the integral bilayer silk scaffold combined with Sil-MA hydrogel in osteochondral repair.

osteochondral engineering (Fig. 1). The physicochemical, mechanical and biological properties of the composite were evaluated in vitro to optimize and construct a bifunctional scaffold and photocurable Sil-MA hydrogel. For bone regeneration, a porous subchondral bone layer loaded with bone morphological protein-2 (BMP-2) could promote fast bone formation. For cartilage regeneration, new cartilage could grow towards and replace the degraded biomimetic cartilage layer from the adjacent cartilage after marginal sealing of the Sil-MA hydrogel. Finally, new osteochondral tissue was regenerated, and integration of the engineered tissue with the native tissue was achieved. Our study proposed a new approach of marginal sealing around integral bilayer scaffolds with Sil-MA hydrogel, which holds great potential for future clinical translation in osteochondral regeneration.

2. Materials and methods

2.1. Fabrication of the bilayer silk scaffold and Sil-MA hydrogel

SF and Sil-MA solutions were prepared as previously described [29]. Briefly, 20 g of sliced cocoons was boiled in 6 L of 0.02 M Na_2CO_3 solution for 30 min at 100 °C to remove the sericin and then washed several times with distilled water. Subsequently, the degummed silk was dried at room temperature and then dissolved in 100 mL of 9.3 M lithium bromide (LiBr) solution at 60 °C for 4 h. Immediately after the SF was dissolved by LiBr, 3 mL (424 mM) of glycidyl methacrylate (GMA) solution (Sigma-Aldrich, St. Louis, USA) was added to 50 mL of the mixture with stirring at 300 rpm for 3 h at 60 °C to create a high-yield reaction between GMA and SF. Then, the resulting solution was centrifuged and dialyzed against distilled water using Slide-A-Lyzer dialysis cassettes (MWCOs of 3500 and 14000 Da for SF and methacrylated SF solutions, respectively) for 2 d. Finally, those solutions were frozen at −80 °C for 12 h and freeze-dried for 48 h. The lyophilized SF and Sil-MA powder were stored at −80 °C for further use.

Bilayer silk scaffolds were prepared as follows. First, different amounts (0.5, 1, and 2 g) of sucrose particles (300–500 μm) were added to 1 mL of hexafluoroisopropanol (HFIP) solution to verify the optimal ratio of 1:1 (Fig. S1). The lyophilized silk powder was dissolved in HFIP without or with sucrose particles to yield 10, 20, and 30% w/v solutions (a dense layer of silk scaffold (D/S) and a porous layer of silk scaffold (P/S)). Two hours after the sucrose particles were mixed with 30% silk-HFIP solution in the silicone mold, 10% silk-HFIP solution was poured onto it. The mixed solution was kept at room temperature overnight for crosslinking into the scaffold state. Then, the demolded scaffold was placed in pure methanol (100% w/v) for 60 min and running water for 24 h to remove the HFIP and sucrose particles. Thus, the upper and lower layers of the bilayer silk scaffold were denoted as the cartilage layer (C layer) and the subchondral bone layer (S layer), respectively.

Photocuring Sil-MA hydrogels were prepared as follows. Lyophilized Sil-MA was dissolved in water at various concentrations from 10 to 30% w/v, and the photoinitiator lithium phenyl(2,4,6-trimethylbenzoyl) phosphinate (LAP) (0.2% w/v) (Tokyo Chemical Industry, Tokyo, Japan) was added and mixed until fully dissolved. The prepared Sil-MA/LAP solution was photocrosslinked via exposure to 30 mW/cm^2 UV light for 30 s at a distance of 5 cm using an Omnicure S2000 (Lumen Dynamics Group).

2.2. Characterization

To compare the microstructure and pore characteristics among the different D/S and P/S groups, scanning electron microscopy (SEM, S-4800, Hitachi, Japan) was performed after the lyophilized samples were flash-frozen in liquid nitrogen, sectioned and gold-coated. In addition, topography and roughness measurements of the cartilage surface and different D/S group samples were performed using an optical profiler (Contour GT-X3, Bruker, Germany). The roughness parameter (arithmetic mean, Ra) of each specimen was measured.

For the mechanical property test, cylindrical D/S and P/S scaffolds (diameter: 10 mm, height: 6 mm) were measured on a universal testing machine (UTM) (HY-0230, Hengyi, China) at a speed of 15 mm/min until 50% deformation of the samples was achieved. The elastic modulus of the scaffolds was calculated from the slope of the stress versus strain curves, limited to the first 10% of the strain.

For better observation of the interface structure, the HFIP solution was mixed with fast-green dye, and the fabricated bilayer scaffold was examined with a stereomicroscope (SZX16; Olympus, Japan) and by SEM.

To determine the methacrylation structure, SF and Sil-MA were examined through ^{1}H nuclear magnetic resonance (^{1}H-NMR) at a frequency of 400 MHz using a Bruker DPX FT-NMR spectrometer (9.4 T, Bruker, Germany) and 700 μL of deuterium oxide (D2O, Sigma-Aldrich) as the solvent per 5 mg of sample. Sil-MA solution was filtered using a 0.45 μm filter before analysis.

A lap shear test was performed to measure the adhesive tensile strength of Sil-MA in conjunction with the cartilage tissue and C layer and the force necessary to separate this bond. One piece of rabbit auricular cartilage (1 cm × 1 cm) and C layer (1 cm × 1 cm) were attached to the edge of the short side of two glass slides (7.6 cm × 2.6 cm). Next, 30 μL of 10% SF and 10–30% w/v Sil-MA solution were uniformly placed on the C layer. Then, the other tissue-coated slide was symmetrically covered with sealants. All groups were irradiated with UV light (30 s) for photocuring. These assembled slides were loaded in a UTM for shear testing by tensile loading with a strain rate of 2 mm/min. The point of detachment was fixed as the maximum load. Shear strength (KPa) was the maximum load (N) divided by the bonding area (1 cm^2).

2.3. Cell viability, attachment, migration and differentiation

The animals used in this research were provided by the Ninth People's Hospital Animal Center (Shanghai, China). All animal protocols were approved by the Animal Care and Experiment Committee of the Ninth People's Hospital.

Four-week-old New Zealand white rabbits were euthanized via an overdose injection of anesthetic and used for the extraction of bone marrow stromal cells (BMSCs) and primary chondrocytes. The cells used in this research were cultured and expanded in high-glucose Dulbecco's modified Eagle's medium (DMEM) (HyClone, USA) supplemented with 10% fetal bovine serum (FBS), 100 U/mL penicillin, and 0.1 mg/mL streptomycin (all from Gibco, USA) and incubated at 37 °C under a 5% CO_2 atmosphere.

BMSCs were extracted from the femurs and tibias of rabbits. After flushing repeatedly with culture medium, the bone marrow suspension was transferred into a culture dish. The culture medium was refreshed every 2 d until approximately 80% confluence was achieved. BMSCs at passages 3–5 were utilized for the in vitro experiments in this study.

Articular cartilage obtained from the femoral heads was used for the extraction of chondrocytes. After mincing into small pieces and digestion with 0.2% collagenase type II for 12 h, the primary chondrocytes were collected and cultivated for two passages before use.

Before cell seeding, the scaffolds were disinfected using 100% ethanol immersion overnight and then lyophilized. Sil-MA solution was sterilized through a 0.45 μm filter. A condensed cell suspension at a density of 2×10^4 BMSCs per P/S sample (diameter of 6 mm, depth of 5 mm) or chondrocytes per 6 cm^2 of D/S sample and Sil-MA hydrogel was seeded on each sample and cultured in an incubator for 2 h. PBS was added to the peripheral wells to avoid liquid evaporation. After cell adherence, culture medium was added for subsequent experiments.

The cell viability of the D/S layer, P/S layer, and Sil-MA hydrogel was examined using a live/dead staining kit (Shanghai Yisheng Biotechnology Co., Ltd., China). BMSCs cultured on the P/S layer and chondrocytes cultured on the D/S layer and Sil-MA hydrogel for 7 d were prepared for the test. After washing with PBS, an assay solution containing calcein-AM and propidium iodide was added to the samples and

incubated at 37 °C for 30 min. The live (green)/dead (red) staining of cells in the scaffolds was observed using a confocal fluorescence microscope (Nikon, Japan). For cell attachment observation, rhodamine-phalloidin and DAPI were applied for cytoskeletal and nuclear staining of cells seeded on the scaffolds.

To test the influence of transforming growth factor-β3 (TGF-β3) released from Sil-MA on the migration of chondrocytes, a Transwell assay was performed. TGF-β3-loaded Sil-MA hydrogel was placed in the lower chambers, and chondrocytes were seeded in the upper chambers. After coculture for 6 h and 12 h, the upper chambers were removed, fixed in 4% paraformaldehyde, and stained with crystal violet. Five random fields of view were selected in each well to count cell numbers.

For the osteogenesis and chondrogenesis tests, BMSCs and chondrocytes seeded on the P/S and D/S layers, respectively, were stimulated with 100 ng/mL BMP-2 (PeproTech, UK) and 20 ng/mL TGF-β3 (PeproTech, UK) for 4, 7, and 14 d. Untreated BMSCs and chondrocytes were used as controls. The gene expression of aggrecan (*Acan*), *Sox9*, and collagen type II (*Col II*) (cartilage-related markers) and of osterix (*Osx*), alkaline phosphatase (*Alp*), and collagen type I (*Col I*) (bone-related markers) was examined using q-PCR analysis with the housekeeping gene *Gapdh* for normalization. The final results were determined using the $2^{-\Delta\Delta Ct}$ method for relative gene expression. The primers utilized in this study were commercially synthesized (Sangon Biotech, Shanghai, China), and the sequences are listed in the supporting information (Table S1).

To further visualize the expression of cartilage-related and bone-related proteins, immunofluorescence staining was used. Primary antibodies against Sox9 and Osx (Abcam, USA) and goat anti-mouse IgG secondary antibodies (Alexa Fluor® 594, Alexa Fluor® 488, Abcam, USA) were used. The cell nuclei were counterstained with DAPI. The images were acquired with a fluorescence microscope.

2.4. In vitro release of BMP-2 and TGF-β3

For growth factor (GF) loading, 200 μg/mL BMP-2 solution was added dropwise onto the S layer of the lyophilized bilayer silk scaffold to the extent that no excess liquid flowed out. Immediately after that, the scaffolds were quickly frozen and lyophilized for subsequent use. TGF-β3 (10 μg/mL) was uniformly mixed with Sil-MA solution and then photocrosslinked under UV light irradiation for 30 s. The above GF-loaded scaffolds were cultured in 1 mL of complete medium. Half the supernatant (500 μL) was collected at different time points (6 h, 12 h, 24 h, 3 d, 5 d, 7 d, 10 d, 14 d, 17 d, and 21 d), followed by the addition of 500 μL of fresh medium. Then, the GFs were measured using enzyme-linked immunosorbent assay (ELISA) kits following the manufacturer's instructions.

2.5. Osteochondral defect repair

All the rabbits (2.5–3.0 kg) were randomly divided into five groups: S layer, BMP-2/S layer, bilayer, BMP-2/bilayer, and BMP-2/bilayer + TGF-β3/Sil-MA (n = 5 for each group). After anesthesia via intravenous injection of 1% pentobarbital sodium (40 mg/kg), a full-thickness osteochondral defect (diameter of 6 mm, depth of 5 mm) was made using an electrical trephine in the articular surface of the femoral patellar groove. Then, the bilayer silk scaffold (6 mm × 5 mm) was implanted into the osteochondral defects. Sil-MA hydrogel was carefully injected into the margins of the cartilage layer and then crosslinked with UV light for 30 s. The wound was closed by suturing the knee joint capsule and the skin layer by layer. The rabbits were allowed to move freely within individual cages. At 0, 3 and 8 weeks post implantation, the rabbits were sacrificed to obtain knee specimens for further assessment.

The fixed specimens at 8 weeks were first photographed and graded blindly by two independent observers in terms of cartilage repair according to the international cartilage repair society (ICRS) scoring system. Afterwards, micro-CT (μCT50, Scanco Medical, Switzerland) analysis was conducted to evaluate bone formation. A cylindrical area with its radius in the center of the defect site was selected as the region of interest (ROI) for the 3D reconstruction and quantification of bone mineral density (BMD), bone volume/tissue volume (BV/TV) and trabecular thickness (Th). After decalcification in 20% EDTA, dehydration, and embedding in paraffin, specimens at 3 and 8 weeks were sliced at a thickness of 4 μm. The sections were stained with safranin-O and fast green for cartilage matrix observation.

For hard tissue sections, the samples at 0 weeks were fixed, dehydrated in gradient ethanol, and embedded in polymethylmethacrylate (PMMA). The samples were cut into sections with a thickness of 150 μm using a Leica SP1600 saw microtome (Leica, Germany), and the sections were polished to a final thickness of approximately 40 μm.

2.6. Statistical analysis

All of the quantitative data are reported as the means ± standard deviations. The statistical analysis was performed using the SPSS 20.0 statistical software package. The groups were compared using one-way analysis of variance (ANOVA) followed by Tukey's post hoc test for multiple comparisons. The levels of significance were established at *P < 0.05 and **P < 0.01. NS denoted not significantly different.

3. Results and discussion

3.1. Bilayer silk scaffold preparation and characterization

For osteochondral engineering, we designed and fabricated an integral bilayer silk scaffold based on the optimized parameters (Fig. 2A). To optimize the parameters of the ultimate bilayer construct, different concentrations (10, 20, and 30% w/v) of D/S and P/S were prepared and characterized. As observed by SEM, D/S manifested a smooth and flat surface with no differences between different groups, while P/S showed a porous structure with collapsed pores in 10% P/S and uniformly interconnected pores of 300–500 μm diameter in 20% and 30% P/S (Fig. 2B). This may result from the weak mechanical strength of 10% P/S, which is not suitable for bone support [30,31]. In addition, we confirmed the mechanical properties by obtaining stress-strain curves for compression (Fig. 2C). The compressive elastic modulus increased with increasing silk concentrations. The 30% P/S group was the strongest, with an elastic modulus of 340 ± 15 KPa (Fig. 2C). Notably, the elastic modulus of the 10% D/S group was 1.25 ± 0.3 MPa, close to that of native cartilage (Fig. 2C) [32]. After compression to 50% deformation, 10% D/S and 30% P/S restored their original shapes immediately, indicating that they possess a degree of elasticity (Fig. S2). Based on the above results, 10% D/S and 30% P/S were preliminarily chosen as candidates. To further confirm 10% D/S as the best candidate, the surface morphology was examined to compare the surface roughness between native cartilage and 10–30% D/S. The results showed that 10% D/S had the roughness value (Ra) most similar to that of native cartilage, and 30% D/S had the lowest roughness value (Fig. 2D). The different roughness values might result from the varying space left by the solvent.

For the cytological experiments, we tested the cell viability, adhesion and differentiation of primary chondrocytes and BMSCs seeded on 10–30% D/S and P/S materials. All the cells were stained green as live cells, indicating the high survival rate of chondrocytes on the scaffold. However, the cell numbers of the 30% D/S group increased less than those of the 10% and 20% D/S groups after 7 d of culture, suggesting that too smooth a surface was not conducive to cell proliferation (Fig. 2E) [33,34]. For all groups, chondrocytes maintained their spherical shape with good attachment to the surface (Fig. S3). After stimulation with TGF-β3 for 4, 7, and 14 d, the expression of cartilage-related markers (*Sox9, Acan, Col II*) was evaluated. The expression of these genes increased with prolonged incubation times, and that in the 30% D/S group increased the least (Fig. 2F). Immunofluorescence staining of

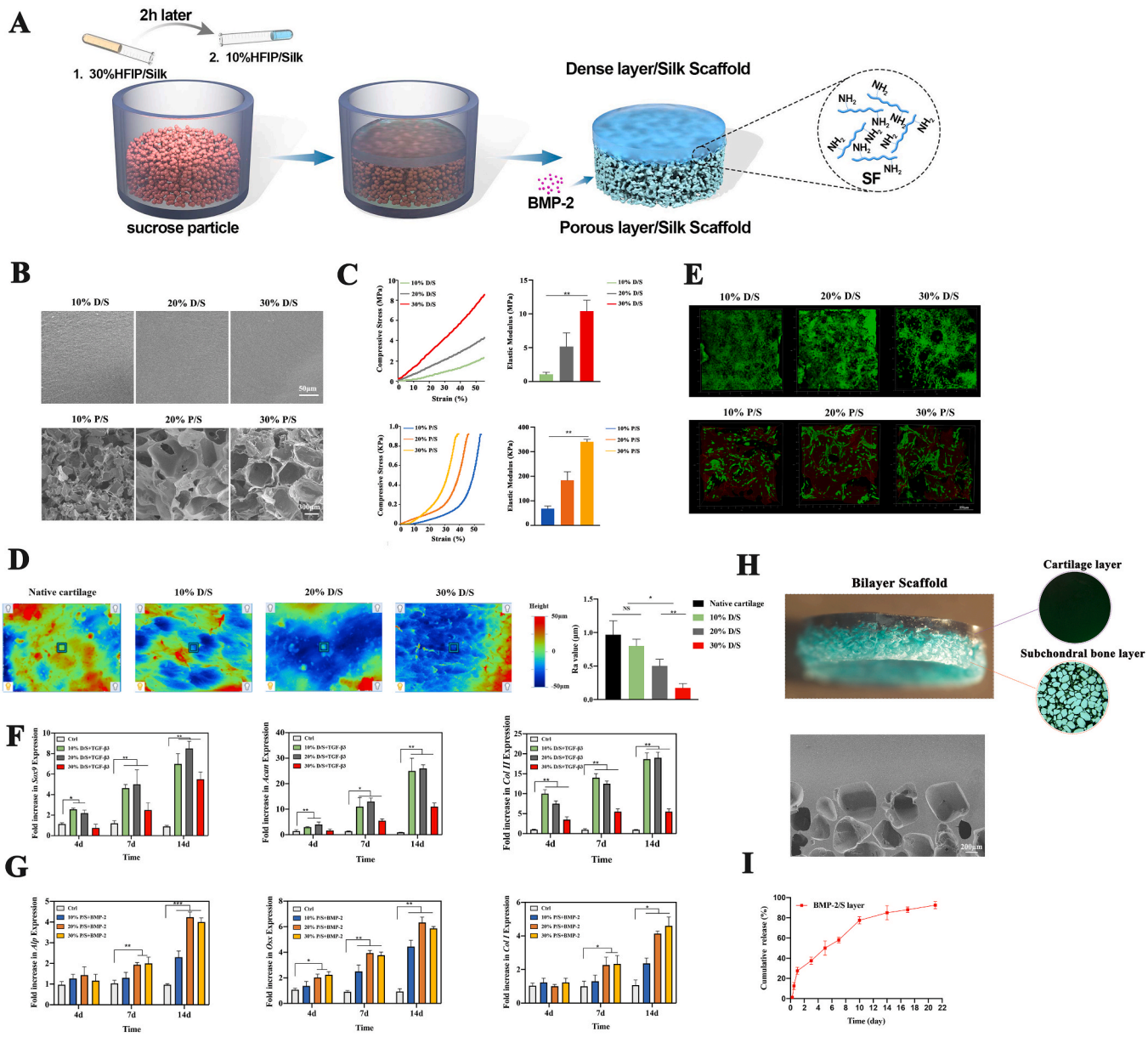

Fig. 2. Bilayer silk scaffold preparation and characterization. A) Illustration of bilayer silk scaffold preparation. B) Morphological observation of all samples, including 10–30% D/S and 10–30% P/S materials. C) Stress-strain curves and elastic modulus of 10–30% D/S and 10–30% P/S materials. D) Surface roughness of native cartilage and 10–30% D/S materials; the value of the representative roughness parameter Ra was quantified. E) Live/dead staining of BMSCs on P/S materials and chondrocytes on D/S materials after 7 d of culture. F) After stimulation with TGF-β3 for 4, 7, and 14 d, the expression of cartilage-related genes (*Sox9, Acan,* and *Col II*) in chondrocytes on D/S materials was evaluated by q-PCR. G) The expression of bone-related genes (*Alp, Osx,* and *Col I*) was examined by q-PCR when BMSCs on P/S materials were cocultured with BMP-2 for 4, 7, and 14 d. H) Stereomicroscopic and SEM images of bilayer silk scaffolds. I) Cumulative release curve of BMP-2 from the subchondral bone layer of the bilayer scaffold.

Sox9 showed that the 10–20% D/S group had higher expression than the 30% D/S group (Fig. S4). These results suggested that 30% D/S group with excessive stiffness and smooth surface is unsuitable for chondrocyte growth and chondrogenesis [35,36]. On the other hand, almost all BMSCs were alive on the P/S materials, verifying the excellent biocompatibility of this scaffold (Fig. 2E). Additionally, cell proliferation and adhesion were enhanced with increasing silk concentrations. In addition, BMSCs on the 30% P/S material grew better and were fully spread, with a spindle shape (Fig. S5). Following coculture with BMP-2 for 4, 7, and 14 d, bone-related genes (*Osx, Alp, Col I*) were highly expressed, except in the 10% P/S group (Fig. 2G). Protein staining of Osx also yielded the same results (Fig. S6). The above investigation illustrated that substrate stiffness mediates differentiation and induces osteogenesis via the mechanical feedback of the ECM anchored to the substrate, as previously observed [37,38].

Thus, the 10% D/S and 30% P/S groups were adopted as the best candidates for the bilayer construct. As indicated in Fig. 2H, this scaffold is an integrated whole consisting of an upper dense layer and a lower porous layer, and the interface observed by SEM showed a natural and continuous connection without cracks. To achieve bone regeneration in vivo, a BMP-loaded (on the S layer) bilayer scaffold was prepared. The cumulative release profiles of BMP-2 showed that the bioactive factor could be sustainably released over an incubation time of 3 weeks (Fig. 2I). After induction with BMP-2, the porous structure with a 300–500 μm diameter facilitated nutrient and tissue ingrowth, achieving fast bone regeneration [39,40].

3.2. Synthesis and characterization of the Sil-MA hydrogel

Recently, Sil-MA has been successfully used externally and internally as a medical glue for hemostasis, promoting tissue healing [41]. The effect relies on the rapid crosslinking, high adhesion and biocompatibility of the Sil-MA hydrogel [42,43]. Inspired by this, we proposed a Sil-MA hydrogel as an adhesive sealant to promote osteochondral healing. Thus, the Sil-MA material was fabricated by methacrylate substitution of the primary amines of SF (Fig. 3A). Modification of GMA on SF was confirmed through identification of GMA-related peaks and SF-related peaks in ^{1}H-NMR spectroscopy (Fig. 3B). Specifically, we found that the characteristic resonance of the methacrylate vinyl group (δ = 6–5.5 ppm) and the methyl group (δ = 1.8 ppm) of GMA appeared upon the addition of GMA.

To make the best choice, the physicochemical and biological properties of the 10–30% Sil-MA hydrogels were evaluated. LAP, which has great water solubility and biocompatibility in vitro and vivo, was added to photopolymerize and form Sil-MA hydrogel [26,29,44]. Compared with primary chondrocytes cultured in normal medium, cells seeded on the 10%, 20% and 30% hydrogels survived perfectly, and a mild aggregation was detected with increasing concentration of Sil-MA due to strong interaction between cells by decreasing pore sizes (Fig. 3C) [29]. Furthermore, 10% SF and 10–30% Sil-MA hydrogels were subjected to a lap shear test to evaluate the strength properties of sealants under tension. As shown in Fig. 3D, the 20% and 30% Sil-MA hydrogels showed higher shear strain and shear stress at break than 10% Sil-MA and 10% SF. Though 30% Sil-MA hydrogel performed best in terms of cell viability and adhesion strength, the factor of degradation rate should be considered. Therefore, the 20% Sil-MA hydrogel was chosen as the best sealant. Fig. 3E shows the adhesion interface between native cartilage and the cartilage layer of the bilayer scaffold with 20% Sil-MA, verifying the tight junction without a gap.

When injected into the gap between the cartilage layer of the scaffold and surrounding tissues, Sil-MA sealant functions as a powerful factor that can guide new cartilage to grow, extend, and rapidly undergo chondrogenesis. Hence, TGF-β3, an indispensable bioactive factor for neocartilage regeneration, was introduced into this hydrogel [45,46]. The cumulative release curve showed that 50% of the TGF-β3 was released after 10 d, and the total increased to 60% after 21 d, indicating that the proteins were encapsulated in the complicated hydrogel networks (Fig. 3F). In addition, a chondrocyte migration assay was performed under the stimulation of the TGF-β3-loaded Sil-MA hydrogel in the lower chamber. At the early 6 h time point, purple-stained cells were found in the TGF-β3/Sil-MA group, while none were found in the control

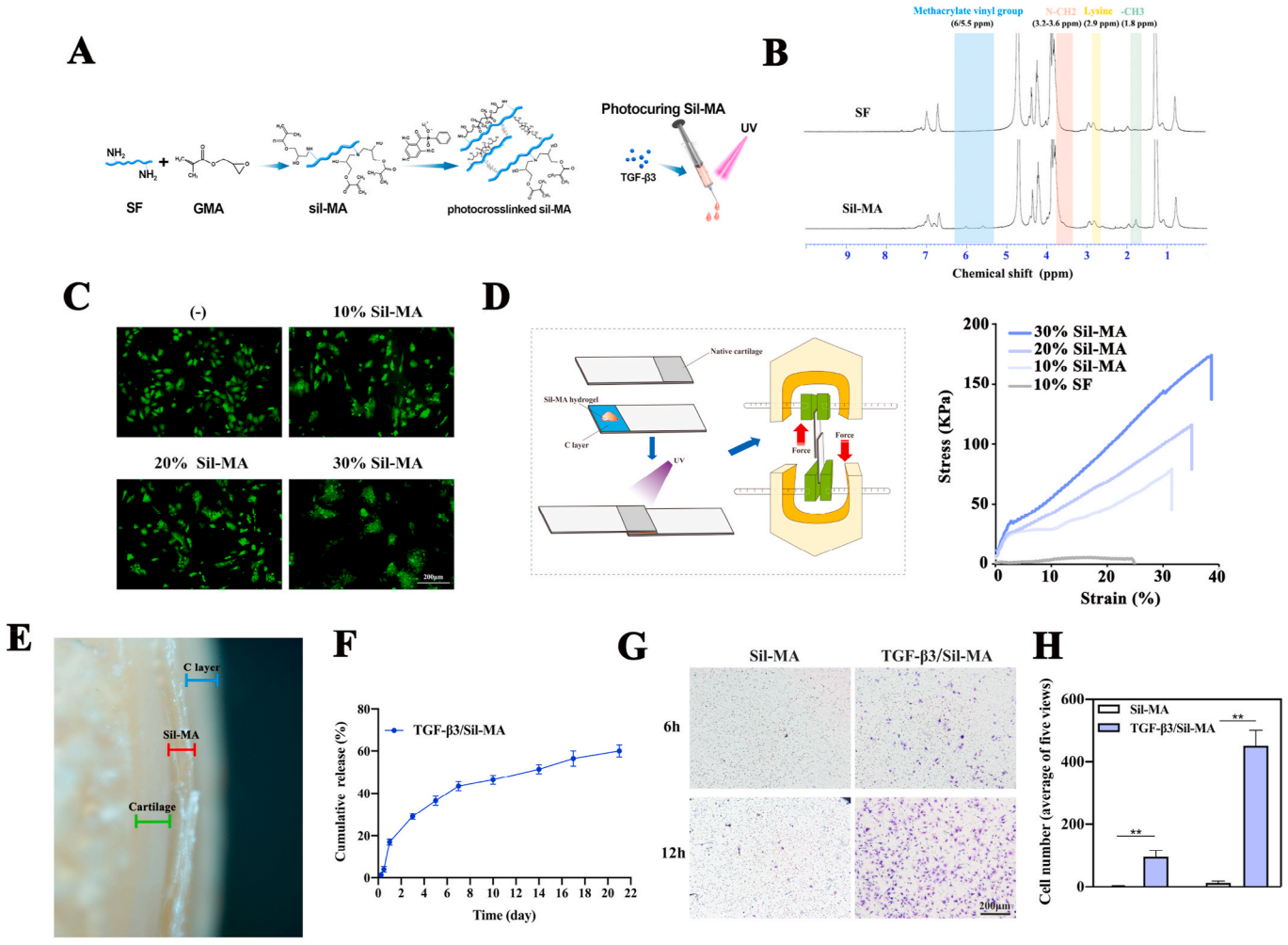

Fig. 3. Synthesis and characterization of the Sil-MA hydrogel. A) Illustration of Sil-MA hydrogel preparation. B) ^{1}H-NMR spectra of SF and Sil-MA. C) Cell viability of chondrocytes on 10–30% Sil-MA compared with primary chondrocytes cultured in normal medium. D) Schematic of the measurement procedure for the strength property relative to lap shear and its representative stress/strain curve of 10% SF, 10–30% Sil-MA. E) Adhesion interface of 20% Sil-MA bonded between native cartilage and the C layer of the bilayer scaffold. Green, red and blue symbols represent the distributions of native cartilage, 20% Sil-MA, and the C layer of the scaffold, respectively. F) Cumulative release curve of TGF-β3 from 20% Sil-MA. G) Transwell assay to test the migration effect of TGF-β3 released from 20% Sil-MA on chondrocytes. H) Migrated cells were quantified by counting.

group. The number of migrated cells increased obviously in the TGF-β3/Sil-MA group, whereas only a few cells appeared in the control group at 12 h (Fig. 3G). The cell counts confirmed the significant differences in the migration of chondrocytes between the TGF-β3/Sil-MA group and the control group (Fig. 3H). TGF-β3 discharged from the Sil-MA hydrogel also enhanced the chondrogenesis of primary chondrocytes seeded on the cartilage layer of the bilayer scaffold, as revealed by q-PCR and immunofluorescence staining (Fig. 2F, S4).

Even though scaffolds designed for knee repair are commonly fabricated with the same size as osteochondral defects made in animals, the two are not precisely matched, which always results in a small gap that hinders rapid and effective neocartilage formation. In this study, the injectable Sil-MA hydrogel loaded with TGF-β3 aimed to adhere the cartilage layer of the scaffold to the surrounding tissue and promote perfect lateral integration. TGF-β3 can promote cartilage regeneration by facilitating the homing of endogenous cells without cell transplantation [47].

3.3. Marginal sealing effect of the Sil-MA hydrogel in vivo

Rabbits were used as animal models to evaluate the knee repair capacity of the bilayer scaffold and Sil-MA hydrogel (Fig. 4A). As illustrated in Fig. 4B, an osteochondral defect was prepared, and blood flowed from the bone marrow cavity, suggesting that the depth of the defect reached the subchondral bone (Fig. 4B–a). When the bilayer scaffold was implanted (Fig. 4B–b), there was still blood oozing from the defect, implying that the scaffold was not tightly fitted to the defect (Fig. 4B–c). However, after injecting the Sil-MA hydrogel into the gap and photocuring by UV irradiation, the bleeding stopped (Fig. 4B–d, e, f) (Video S1). This phenomenon indicated that the Sil-MA hydrogel successfully sealed the cartilage layer of the scaffold and the surrounding tissue. It is believed that Sil-MA's strong adhesive properties result from a combination of mechanical interlocking by the penetration of Sil-MA solution into the irregular tissue surface and C layer surface [48] and covalent bonding of the radicals generated during the photopolymerization process [49]. Additionally, the hydrophobic/hydrophilic interactions and electrostatic interactions between the tissue surface (C layer surface) and Sil-MA solution would increase adhesion. The adhesion mechanism of Sil-MA has not been clarified and requires further study.

Supplementary data related to this article can be found at https://doi.org/10.1016/j.bioactmat.2021.04.005.

To clarify the specific effect of the Sil-MA hydrogel on osteochondral regeneration, the repair conditions at different time points (0 and 3 weeks) were observed (Fig. 4C). At the implantation site, the C layer was bonded closely with the adjacent cartilage by the Sil-MA hydrogel in the bilayer + Sil-MA group, while there was still a gap between the C layer and the adjacent cartilage in the bilayer group at high power. After 3 weeks, newly formed cartilage filled the whole defect, growing along the surface of the C layer and replacing it gradually with new cartilage as the scaffold degraded in the bilayer + Sil-MA group. However, neocartilage had just begun to extend to the margin of the defect of the adjacent cartilage without the Sil-MA sealant. These results proved the effect of the Sil-MA hydrogel on the integration of the cartilage layer of the scaffold with native cartilage and the promotion of rapid cartilage formation.

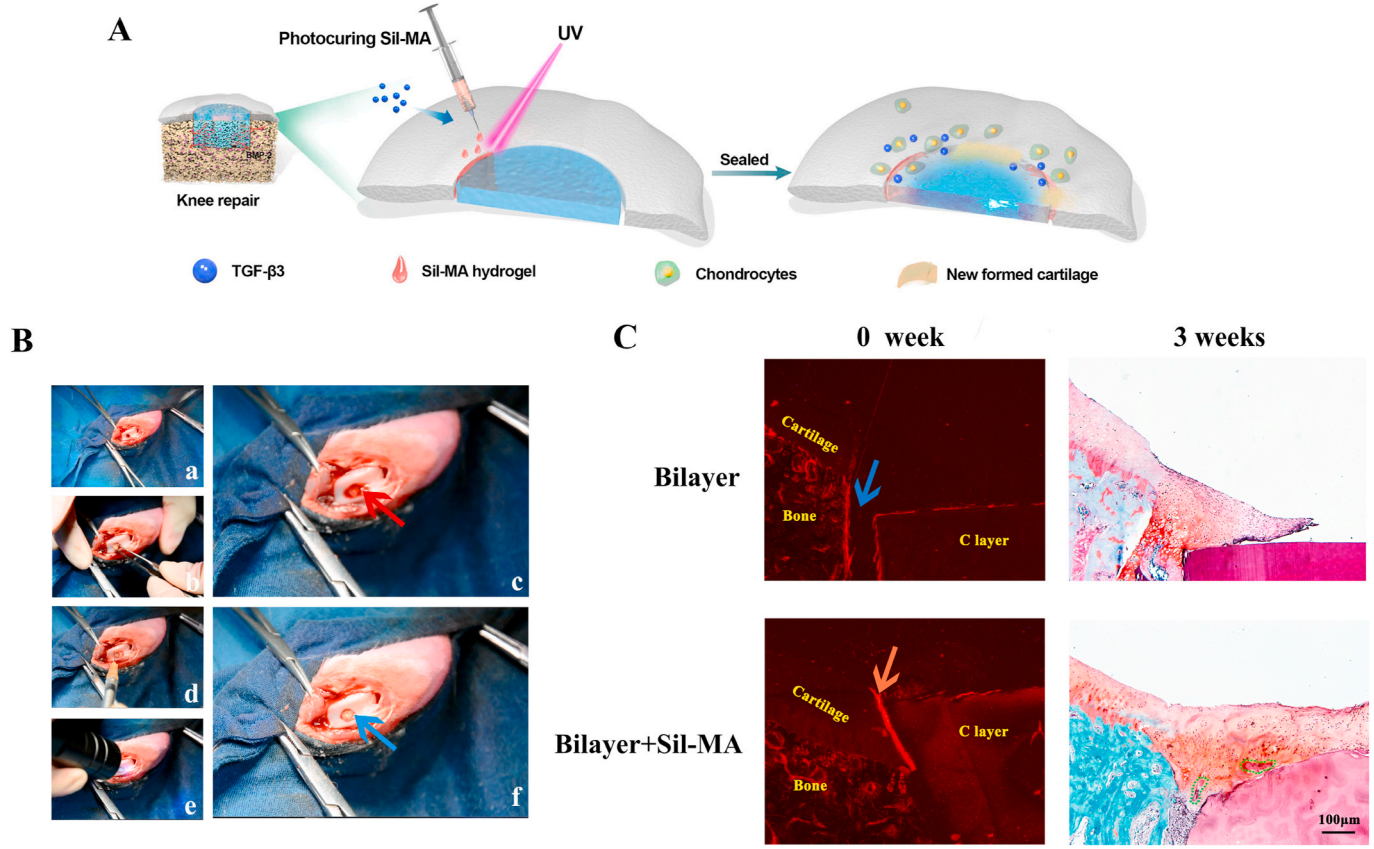

Fig. 4. Marginal sealing effect of the Sil-MA hydrogel in vivo. A) Procedures for Sil-MA hydrogel application. B) Surgical procedures for the use of bilayer silk scaffolds combined with Sil-MA hydrogel in osteochondral repair: a) defect preparation; b) scaffold implantation; c) bleeding; d) 20% Sil-MA hydrogel injection; e) UV irradiation; f) stopped bleeding and completion. The red arrow indicates blood flowing from the defect after scaffold implantation. The blue arrow shows that the bleeding stopped after Sil-MA hydrogel application. C) Immediate implantation conditions at 0 weeks and repair conditions at 3 weeks were observed to evaluate the effect of the Sil-MA hydrogel. The blue arrow represents the gap between the C layer and native cartilage. The red arrow indicates the tight link between the C layer and native cartilage sealed by the 20% Sil-MA hydrogel. Green irregular shapes point to the undegraded C layer material that is replaced with neocartilage.

A biologically active, high-strength tissue adhesive for cartilage tissue-scaffold integration is needed in osteochondral engineering. On one hand, it is important for the initial stability of the implanted scaffold and efficient load transfer, which benefit tissue repair at early stage; on the other hand, it is crucial for the integration of scaffold-guided neocartilage with surrounding native cartilage [50]. Previously, researchers reported the use of chondroitin sulphate or M-*O*-G (composed of gelatin methacrylate, oxidized dextran, and gelatin) adhesives for hydrogel-based cartilage repair [51,52]. However, a hydrogel scaffold alone is inadequate for cartilage regeneration due to its weak mechanical strength, and adhesives with limited adhesive strength are insufficient for silk scaffold-based cartilage repair.

In this work, we proposed Sil-MA hydrogel as a marginal sealant for a bilayer silk scaffold, taking advantage of its good biocompatibility, high adhesive strength, and excellent adherence and integration with the surrounding native cartilage. According to the reasons for difficulty in achieving lateral integration, the new approach of Sil-MA sealant combined with bilayer scaffold mainly focuses on these aspects: 1) Sil-MA hydrogel directly adheres the cartilage layer of the scaffold and adjacent cartilage together to promote stable scaffold fixation; 2) neocartilage formation relies on endogenous cells, for example, cartilage progenitor cells; and 3) the cartilage layer of the scaffold is designed resembling native cartilage in surface morphology and mechanical strength.

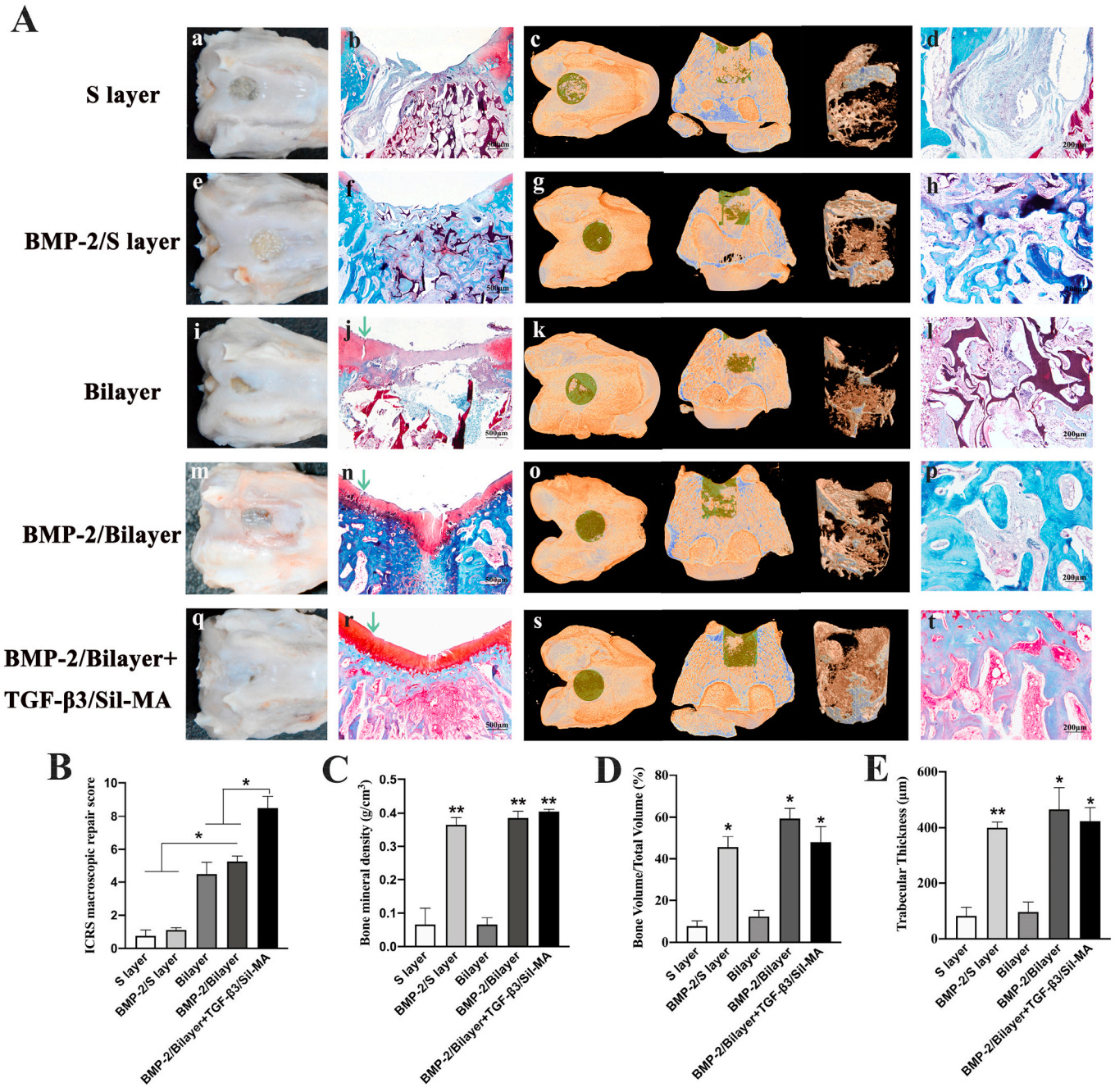

Fig. 5. Osteochondral engineering using the all-silk-derived composite. A) a, e, i, m, q, Gross images of different groups. c, g, k, o, s, Micro-CT 3D images of different groups. The dark yellow, green and brown colors in the 3D reconstruction images represent the primary bone, new bone and 3D reconstructed new bone, respectively, within the selected ROI. b, f, j, n, r, d, h, l, p, t, Histological analysis of different groups by safranin-O/fast-green staining. The green arrows in Fig. 5A–j, n, and r indicate lateral integration between neocartilage and adjacent cartilage. B) The ICRS macroscopic repair scores were quantified. C) BMD (g/cm^3), D) BV/TV (%) and E) Th (μm) values of micro-CT bone remodeling were quantitatively measured.

3.4. Osteochondral engineering using the all-silk-derived composite

The potential of the all-silk-derived composite for knee repair was further evaluated after 8 weeks of healing. The regenerative capability of osteochondral tissues was assessed by gross evaluation, micro-CT, and histologic analyses. In a conventional cartilage characterization method, histological sections were stained with Safranin-O, which dyes glycosaminoglycan (GAG) red to identify cartilage tissue. In addition, fast-green integrates with collagen fibers and can dye bone tissues green or blue to distinguish bone from cartilage. In the S layer group, flattened tissue steps could be observed within the defect, indicating poor chondrogenesis (Fig. 5A–a). Neither safranin-O staining nor obvious newly formed bone was observed in the osteochondral defect. Only incompletely degraded high-density material with fibrous connective tissue ingrowth was observed (Fig. 5A–b, c, d). This result suggests that the porous silk material alone has no osteogenic or chondrogenic capacity and should be combined with bioactive factors to promote osteochondral regeneration [19,23,53]. Hence, the BMP-2/S layer group surpassed the S layer group in terms of the appearance of bone repair, which was attributed to the powerful osteogenic stimulator BMP-2, and a substantial amount of well-arranged new bone was observed to fill the whole defect (Fig. 5A–f, g, h). Then, we constructed a bilayer scaffold with high density, a slightly smooth surface, some degree of stiffness, a biomimetic cartilage layer and a porous subchondral bone layer for osteochondral repair. In the bilayer group, half of the defect was covered with whitish tissues, which had a tight connection with the underlying cartilage layer material (Fig. 5A–i). It could be inferred that the newly regenerated tissue generally grew from the margin of the defects to the top and center. Histologically, the newly formed cartilage was thin and obviously not integrated with the adjoining cartilage (Fig. 5A–j). In addition, scarce bone formation was found at the bottom edge of the defect, which was speculated to be intrinsically repaired without the influence of BMP-2 (Fig. 5A–j, k, l). Moreover, in the BMP-2/bilayer group, the treated area was nearly wrapped with white, translucent tissues, still distinguishable from the normal cartilage (Fig. 5A-m). The histological examination showed complete osseous filling, with a top layer of cartilage-like tissue in the specimens (Fig. 5A-n, p). Unfortunately, there was a crack between the new tissues and the adjoining cartilage (Fig. 5A-n). The results revealed that the biomimetic design of the cartilage layer benefited chondrocyte growth and regeneration, even though the structure, morphology and lateral integration with native cartilage were not ideal.

Therefore, a TGF-β3-loaded Sil-MA hydrogel was added to assist the BMP-2/bilayer scaffold. After 8 weeks, smooth, consistent and white opaque tissues were observed in the regenerated area (Fig. 5A-q). The μ-CT reconstruction images showed that the subchondral bone defect was filled with newly regenerated bone tissue, and the new bone mainly regenerated from the edge of the defect towards the center (Fig. 5A–s). Histologically, compact, continuous neocartilage was observed to be well interconnected with the adjoining cartilage. In addition, good reconstitution of subchondral bone and mature trabecular bone ingrowth within the subchondral region were observed, with good integration into the native bone tissue and no visible demarcation (Fig. 5A-r, t). Thus, the BMP-2/bilayer + TGF-β3/Sil-MA group showed better performance for osteochondral defect repair than the BMP-2/bilayer group.

The ICRS scores (indicative of neocartilage) were apparently higher in the bilayer, BMP-2/bilayer and BMP-2/bilayer + TGF-β3/Sil-MA groups than the S layer and BMP-2/S layer groups, and highest score was found in the BMP-2/bilayer + TGF-β3/Sil-MA groups (Fig. 5B). In addition, quantitative evaluation of the newly formed bone within the defect verified the above observations. These measurements revealed that the values of BMD, BV/TV and Th in the trabecular volume of interest were significantly higher in the BMP-2/S layer, BMP-2/bilayer and BMP-2/bilayer + TGF-β3/Sil-MA groups than in the other two groups, which suggests that incorporating BMP-2 into the porous silk layer enhanced the bone regenerative ability (Fig. 5C–E).

Overall, the BMP-2/bilayer + TGF-β3/Sil-MA group exhibited optimal osteochondral defect repair in several respects: 1) the combination of BMP-2 and a porous structure promoted rapid bone formation; 2) the designed biomimetic cartilage layer facilitated chondrocyte growth and regeneration; and 3) the TGF-β3-loaded Sil-MA hydrogel sealed the marginal gap between the cartilage layer of the scaffold and native cartilage, accelerating lateral integration.

4. Conclusions

In summary, an integral bilayer silk scaffold consisting of a dense, smooth, biomimetic cartilage layer and a BMP-2-loaded porous layer combined with TGF-β3/Sil-MA sealant was successfully constructed for osteochondral repair. For bone regeneration, the BMP-2-loaded interconnected 3D porous network benefits nutrient and tissue ingrowth, provides excellent mechanical properties to support newly formed tissue, and stimulates the osteogenic differentiation of BMSCs. For cartilage regeneration, the cartilage layer facilitates chondrocyte growth and regeneration and lateral integration with the adjoining cartilage sealed by the TGF-β3/Sil-MA hydrogel. This composite achieves osteochondral repair by using endogenous cells. Due to its excellent lateral integration and its other outstanding properties, this composite design has been demonstrated to be a potential scaffold for osteochondral repair and to be worthy of further investigation to facilitate clinical application.

CRediT authorship contribution statement

Xiaolin Wu: Conceptualization, Methodology, Writing – original draft. **Mingliang Zhou:** Conceptualization, Resources, Writing – review & editing. **Fei Jiang:** Visualization, Formal analysis, Data curation. **Shi Yin:** Validation, Data curation. **Sihan Lin:** Software, Investigation. **Guangzheng Yang:** Data curation, Software. **Yuezhi Lu:** Resources, Supervision. **Wenjie Zhang:** Resources, Writing – review & editing, Supervision. **Xinquan Jiang:** Conceptualization, Writing – review & editing, Funding acquisition.

Declaration of competing interest

The authors declare that they have no known competing financial interests or personal relationships that could have appeared to influence the work reported in this paper.

Acknowledgments

This work was jointly supported by the National Natural Science Foundation of China (No. 81921002, 81620108006, 81991505, 31700848) and the National Key Research and Development Program of China (2016YFC1102900). The authors gratefully acknowledge the Innovative Research Team of High-level Local Universities in Shanghai, Oral and Maxillofacial Regeneration and Functional Restoration.

Appendix A. Supplementary data

Supplementary data to this article can be found online at https://doi.org/10.1016/j.bioactmat.2021.04.005.

References

[1] J.S. TemenoffA, G. Mikos, Review: tissue engineering for regeneration of articular cartilage, Biomaterials 21 (5) (2000) 431–440, https://doi.org/10.1016/s0142-9612(99)00213-6.

[2] D.J. Huey, J.C. HuK, A. Athanasiou, Unlike bone, cartilage regeneration remains elusive, Science 338 (6109) (2012) 917–921, https://doi.org/10.1126/science.1222454.

[3] J.P.K. Armstrong, R. Shakur, J.P. Horne, S.C. Dickinson, C.T. Armstrong, K. Lau, J. Kadiwala, R. Lowe, A. Seddon, S. Mann, J.L.R. Anderson, A.W. PerrimanA, P. Hollander, Artificial membrane-binding proteins stimulate oxygenation of stem

cells during engineering of large cartilage tissue, Nat. Commun. 6 (2015) 7405, https://doi.org/10.1038/ncomms8405.
[4] L. Zhou, V.O. Gjvm, J. Malda, M.J. Stoddart, Y. Lai, R.G. Richards, K. Ki-Wai Ho, L. Qin, Innovative tissue-engineered strategies for osteochondral defect repair and regeneration: current progress and challenges, Adv. Healthc. Mater. (2020), https://doi.org/10.1002/adhm.202001008 e2001008.
[5] L. Li, J. Li, J. Guo, H. Zhang, X. Zhang, C. Yin, L. Wang, Y. ZhuQ. Yao, 3D molecularly functionalized cell-free biomimetic scaffolds for osteochondral regeneration, Adv. Funct. Mater. 29 (6) (2019) 1807356, https://doi.org/10.1002/adfm.201807356.
[6] Y. Zhang, X. Liu, L. Zeng, J. Zhang, J. Zuo, J. Zou, J. DingX. Chen, Polymer fiber scaffolds for bone and cartilage tissue engineering, Adv. Funct. Mater. 29 (36) (2019), https://doi.org/10.1002/adfm.201903279.
[7] X. Liu, Y. Wei, C. Xuan, L. Liu, C. Lai, M. Chai, Z. Zhang, L. WangX. Shi, A biomimetic biphasic osteochondral scaffold with layer-specific release of stem cell differentiation inducers for the reconstruction of osteochondral defects, Adv. Healthc. Mater. (2020), https://doi.org/10.1002/adhm.202000076 e2000076.
[8] I.M. Khan, S.J. Gilbert, S.K. Singhrao, V.C. DuanceC, W. Archer, Cartilage integration: evaluation of the reasons for failure of integration during cartilage repair. A review, Eur. Cell. Mater. 16 (2008) 26–39, https://doi.org/10.22203/ecm.v016a04.
[9] S.P.J. Miguel Oliveira, Rui L. Reis, Julio San Roman, Osteochondral Tissue Engineering, first ed., Springer, Cham, 2018.
[10] D. He, D.G. Genecov, M. Herbert, R. Barcelo, M.E. Elsalanty, B.E. WeprinL, A. Opperman, Effect of recombinant human bone morphogenetic protein-2 on bone regeneration in large defects of the growing canine skull after dura mater replacement with a dura mater substitute, J. Neurosurg. 112 (2) (2010) 319–328, https://doi.org/10.3171/2009.1.Jns08976.
[11] Z. Qiao, M. Lian, Y. Han, B. Sun, X. Zhang, W. Jiang, H. Li, Y. HaoK. Dai, Bioinspired stratified electrowritten fiber-reinforced hydrogel constructs with layer-specific induction capacity for functional osteochondral regeneration, Biomaterials 266 (2021) 120385, https://doi.org/10.1016/j.biomaterials.2020.120385.
[12] H. Zhang, H. Huang, G. Hao, Y. Zhang, H. Ding, Z. FanL. Sun, 3D printing hydrogel scaffolds with nanohydroxyapatite gradient to effectively repair osteochondral defects in rats, Adv. Funct. Mater. 31 (1) (2021) 2006697, https://doi.org/10.1002/adfm.202006697.
[13] J. van de Breevaart Bravenboer, C.D. In der Maur, P.K. Bos, L. Feenstra, J. A. Verhaar, H. WeinansG, J. van Osch, Improved cartilage integration and interfacial strength after enzymatic treatment in a cartilage transplantation model, Arthritis Res. Ther. 6 (5) (2004) R469–476, https://doi.org/10.1186/ar1216.
[14] C. Englert, K.B. McGowan, T.J. Klein, A. Giurea, B.L. SchumacherR, L. Sah, Inhibition of integrative cartilage repair by proteoglycan 4 in synovial fluid, Arthritis Rheum. 52 (4) (2005) 1091–1099, https://doi.org/10.1002/art.20986.
[15] S.J. Gilbert, S.K. Singhrao, I.M. Khan, L.G. Gonzalez, B.M. Thomson, D. Burdon, V. C. DuanceC, W. Archer, Enhanced tissue integration during cartilage repair in vitro can be achieved by inhibiting chondrocyte death at the wound edge, Tissue Eng. 15 (7) (2009) 1739–1749, https://doi.org/10.1089/ten.tea.2008.0361.
[16] B. Kuang, Y. YangH. Lin, Infiltration and in-tissue polymerization of photocross-linked hydrogel for effective fixation of implants into cartilage-an in vitro study, ACS Omega 4 (20) (2019) 18540–18544, https://doi.org/10.1021/acsomega.9b02270.
[17] A.A. Allon, K.W. Ng, S. Hammoud, B.H. Russell, C.M. Jones, J.J. Rivera, J. Schwartz, M. HookS, A. Maher, Augmenting the articular cartilage-implant interface: functionalizing with a collagen adhesion protein, J. Biomed. Mater. Res. 100 (8) (2012) 2168–2175, https://doi.org/10.1002/jbm.a.34144.
[18] V.P. Ribeiro, S. Pina, J.B. Costa, I.F. Cengiz, L. García-Fernández, M.D. M. Fernández-Gutiérrez, O.C. Paiva, A.L. Oliveira, J. San-Román, J.M. OliveiraR, L. Reis, Enzymatically cross-linked silk fibroin-based hierarchical scaffolds for osteochondral regeneration, ACS Appl. Mater. Interfaces 11 (4) (2019) 3781–3799, https://doi.org/10.1021/acsami.8b21259.
[19] Z. Luo, L. Jiang, Y. Xu, H. Li, W. Xu, S. Wu, Y. Wang, Z. Tang, Y. LvL. Yang, Mechano growth factor (MGF) and transforming growth factor (TGF)-β3 functionalized silk scaffolds enhance articular hyaline cartilage regeneration in rabbit model, Biomaterials 52 (2015) 463–475, https://doi.org/10.1016/j.biomaterials.2015.01.001.
[20] B. Kundu, R. Rajkhowa, S.C. KunduX. Wang, Silk fibroin biomaterials for tissue regenerations, Adv. Drug Deliv. Rev. 65 (4) (2013) 457–470, https://doi.org/10.1016/j.addr.2012.09.043.
[21] X. Wang, X. Song, T. Li, J. Chen, G. Cheng, L. YangC. Chen, Aptamer-Functionalized bioscaffold enhances cartilage repair by improving stem cell recruitment in osteochondral defects of rabbit knees, Am. J. Sports Med. 47 (10) (2019) 2316–2326, https://doi.org/10.1177/0363546519856355.
[22] G. Xu, Z. Ding, Q. Lu, X. Zhang, X. Zhou, L. Xiao, G. LuD, L. Kaplan, Electric field-driven building blocks for introducing multiple gradients to hydrogels, Protein Cell 11 (4) (2020) 267–285, https://doi.org/10.1007/s13238-020-00692-z.
[23] Y. Chen, T. Wu, S. Huang, C.W. Suen, X. Cheng, J. Li, H. Hou, G. She, H. Zhang, H. Wang, X. ZhengZ. Zha, Sustained release SDF-1α/TGF-β1-loaded silk fibroin-porous gelatin scaffold promotes cartilage repair, ACS Appl. Mater. Interfaces 11 (16) (2019) 14608–14618, https://doi.org/10.1021/acsami.9b01532.
[24] W. Zhang, C. Ling, A. Zhang, H. Liu, Y. Jiang, X. Li, R. Sheng, Q. YaoJ. Chen, An all-silk-derived functional nanosphere matrix for sequential biomolecule delivery and in situ osteochondral regeneration, Bioact. Mater. 5 (4) (2020) 832–843, https://doi.org/10.1016/j.bioactmat.2020.05.003.
[25] J.J. Li, K. Kim, S.I. Roohani-Esfahani, J. Guo, D.L. KaplanH. Zreiqat, A biphasic scaffold based on silk and bioactive ceramic with stratified properties for osteochondral tissue regeneration, J. Mater. Chem. B 3 (26) (2015) 5361–5376, https://doi.org/10.1039/c5tb00353a.
[26] H. Hong, Y.B. Seo, D.Y. Kim, J.S. Lee, Y.J. Lee, H. Lee, O. Ajiteru, M.T. Sultan, O. J. Lee, S.H. KimC, H. Park, Digital light processing 3D printed silk fibroin hydrogel for cartilage tissue engineering, Biomaterials 232 (2020) 119679, https://doi.org/10.1016/j.biomaterials.2019.119679.
[27] L. Xu, S. Gao, R. Zhou, F. Zhou, Y. QiaoD. Qiu, Bioactive pore-forming bone adhesives facilitating cell ingrowth for fracture healing, Adv. Mater. 32 (10) (2020), https://doi.org/10.1002/adma.201907491 e1907491.
[28] J. Chen, D. Wang, L.H. Wang, W. Liu, A. Chiu, K. Shariati, Q. Liu, X. Wang, Z. Zhong, J. Webb, R.E. Schwartz, N. BouklasM. Ma, An adhesive hydrogel with "Load-Sharing" effect as tissue bandages for drug and cell delivery, Adv. Mater. 32 (43) (2020), e2001628, https://doi.org/10.1002/adma.202001628.
[29] S.H. Kim, Y.K. Yeon, J.M. Lee, J.R. Chao, Y.J. Lee, Y.B. Seo, M.T. Sultan, O.J. Lee, J. S. Lee, S.I. Yoon, I.S. Hong, G. Khang, S.J. Lee, J.J. YooC, H. Park, Precisely printable and biocompatible silk fibroin bioink for digital light processing 3D printing, Nat. Commun. 9 (1) (2018) 1620, https://doi.org/10.1038/s41467-018-03759-y.
[30] E.S. Gil, J.A. Kluge, D.N. Rockwood, R. Rajkhowa, L. Wang, X. WangD, L. Kaplan, Mechanical improvements to reinforced porous silk scaffolds, J. Biomed. Mater. Res. 99 (1) (2011) 16–28, https://doi.org/10.1002/jbm.a.33158.
[31] L. Zhang, G. Yang, B.N. JohnsonX. Jia, Three-dimensional (3D) printed scaffold and material selection for bone repair, Acta Biomater. 84 (2019) 16–33, https://doi.org/10.1016/j.actbio.2018.11.039.
[32] C.J. Little, N.K. BawolinX. Chen, Mechanical properties of natural cartilage and tissue-engineered constructs, Tissue Eng. B Rev. 17 (4) (2011) 213–227, https://doi.org/10.1089/ten.TEB.2010.0572.
[33] B.D. Boyan, T.W. Hummert, D.D. Dean, Z. Schwartz, Role of material surfaces in regulating bone and cartilage cell response, Biomaterials 17 (2) (1996) 137–146, https://doi.org/10.1016/0142-9612(96)85758-9.
[34] B.D. Boyan, J. Lincks, C.H. Lohmann, V.L. Sylvia, D.L. Cochran, C.R. Blanchard, D. D. Dean, Z. Schwartz, Effect of surface roughness and composition on costochondral chondrocytes is dependent on cell maturation state, J. Orthop. Res. 17 (3) (1999) 446–457, https://doi.org/10.1002/jor.1100170322.
[35] J. Lee, O. Jeon, M. Kong, A.A. Abdeen, J.Y. Shin, H.N. Lee, Y.B. Lee, W. Sun, P. Bandaru, D.S. Alt, K. Lee, H.J. Kim, S.J. Lee, S. Chaterji, S.R. Shin, E. AlsbergA. Khademhosseini, Combinatorial screening of biochemical and physical signals for phenotypic regulation of stem cell-based cartilage tissue engineering, Sci. Adv. 6 (21) (2020), https://doi.org/10.1126/sciadv.aaz5913 eaaz5913.
[36] W. Kosorn, M. Sakulsumbat, T. Lertwimol, B. Thavornyutikarn, P. Uppanan, S. ChantaweroadW. Janvikul, Chondrogenic phenotype in responses to poly (ϵ-caprolactone) scaffolds catalyzed by bioenzymes: effects of surface topography and chemistry, J. Mater. Sci. Mater. Med. 30 (12) (2019) 128, https://doi.org/10.1007/s10856-019-6335-6.
[37] J.H. Wen, L.G. Vincent, A. Fuhrmann, Y.S. Choi, K.C. Hribar, H. Taylor-Weiner, S. ChenA, J. Engler, Interplay of matrix stiffness and protein tethering in stem cell differentiation, Nat. Mater. 13 (10) (2014) 979–987, https://doi.org/10.1038/nmat4051.
[38] B. Trappmann, J.E. Gautrot, J.T. Connelly, D.G. Strange, Y. Li, M.L. Oyen, M. A. Cohen Stuart, H. Boehm, B. Li, V. Vogel, J.P. Spatz, F.M. WattW, T. Huck, Extracellular-matrix tethering regulates stem-cell fate, Nat. Mater. 11 (7) (2012) 642–649, https://doi.org/10.1038/nmat3339.
[39] R.K. Jain, P. Au, J. Tam, D.G. Duda, D. Fukumura, Engineering vascularized tissue, Nat. Biotechnol. 23 (7) (2005) 821–823, https://doi.org/10.1038/nbt0705-821.
[40] R. Nazarov, H.J. JinD, L. Kaplan, Porous 3-D scaffolds from regenerated silk fibroin, Biomacromolecules 5 (3) (2004) 718–726, https://doi.org/10.1021/bm034327e.
[41] S.H. Kim, Y.J. Lee, J.R. Chao, D.Y. Kim, M.T. Sultan, H.J. Lee, J.M. Lee, J.S. Lee, O. J. Lee, H. Hong, H. Lee, O. Ajiteru, Y.J. Suh, H.S. Choi, Y.-J. ChoC, H. Park, Rapidly photocurable silk fibroin sealant for clinical applications, NPG Asia Mater. 12 (1) (2020) 46, https://doi.org/10.1038/s41427-020-0227-6.
[42] H. Hong, O.J. Lee, Y.J. Lee, J.S. Lee, O. Ajiteru, H. Lee, Y.J. Suh, M.T. Sultan, S. H. KimC, H. Park, Cytocompatibility of modified silk fibroin with glycidyl methacrylate for tissue engineering and biomedical applications, Biomolecules 11 (1) (2020), https://doi.org/10.3390/biom11010035.
[43] S.H. Kim, Y.B. Seo, Y.K. Yeon, Y.J. Lee, H.S. Park, M.T. Sultan, J.M. Lee, J.S. Lee, O. J. Lee, H. Hong, H. Lee, O. Ajiteru, Y.J. Suh, S.H. Song, K.H. LeeC, H. Park, 4D-bioprinted silk hydrogels for tissue engineering, Biomaterials 260 (2020) 120281, https://doi.org/10.1016/j.biomaterials.2020.120281.
[44] B.D. Fairbanks, M.P. Schwartz, C.N. BowmanK, S. Anseth, Photoinitiated polymerization of PEG-diacrylate with lithium phenyl-2,4,6-trimethylbenzoylphosphinate: polymerization rate and cytocompatibility, Biomaterials 30 (35) (2009) 6702–6707, https://doi.org/10.1016/j.biomaterials.2009.08.055.
[45] R.L. Dahlin, M. Ni, V.V. Meretoja, F.K. KasperA, G. Mikos, TGF-β3-induced chondrogenesis in co-cultures of chondrocytes and mesenchymal stem cells on biodegradable scaffolds, Biomaterials 35 (1) (2014) 123–132, https://doi.org/10.1016/j.biomaterials.2013.09.086.
[46] B. Mohanraj, G. Duan, A. Peredo, M. Kim, F. Tu, D. Lee, G.R. DodgeR, L. Mauck, Mechanically-activated microcapsules for 'on-demand' drug delivery in dynamically loaded musculoskeletal tissues, Adv. Funct. Mater. 29 (15) (2019), https://doi.org/10.1002/adfm.201807909.
[47] C.H. Lee, J.L. Cook, A. Mendelson, E.K. Moioli, H. YaoJ, J. Mao, Regeneration of the articular surface of the rabbit synovial joint by cell homing: a proof of concept study, Lancet 376 (9739) (2010) 440–448, https://doi.org/10.1016/s0140-6736(10)60668-x.

[48] C. GhobrilM, W. Grinstaff, The chemistry and engineering of polymeric hydrogel adhesives for wound closure: a tutorial, Chem. Soc. Rev. 44 (7) (2015) 1820–1835, https://doi.org/10.1039/c4cs00332b.
[49] N. Lang, M.J. Pereira, Y. Lee, I. Friehs, N.V. Vasilyev, E.N. Feins, K. Ablasser, E. D. O'Cearbhaill, C. Xu, A. Fabozzo, R. Padera, S. Wasserman, F. Freudenthal, L. S. Ferreira, R. Langer, J.M. KarpP, J. del Nido, A blood-resistant surgical glue for minimally invasive repair of vessels and heart defects, Sci. Transl. Med. 6 (218) (2014), https://doi.org/10.1126/scitranslmed.3006557, 218ra216.
[50] K.L. Spiller, S.A. MaherA, M. Lowman, Hydrogels for the repair of articular cartilage defects, Tissue Eng. B Rev. 17 (4) (2011) 281–299, https://doi.org/10.1089/ten.TEB.2011.0077.
[51] F. Zhou, Y. Hong, X. Zhang, L. Yang, J. Li, D. Jiang, V. Bunpetch, Y. Hu, H. OuyangS. Zhang, Tough hydrogel with enhanced tissue integration and in situ forming capability for osteochondral defect repair, Appl. Mater. Today 13 (2018) 32–44, https://doi.org/10.1016/j.apmt.2018.08.005.
[52] D.A. Wang, S. Varghese, B. Sharma, I. Strehin, S. Fermanian, J. Gorham, D. H. Fairbrother, B. CascioJ, H. Elisseeff, Multifunctional chondroitin sulphate for cartilage tissue-biomaterial integration, Nat. Mater. 6 (5) (2007) 385–392, https://doi.org/10.1038/nmat1890.
[53] T. Wu, Y. Chen, W. Liu, K.L. Tong, C.W. Suen, S. Huang, H. Hou, G. She, H. Zhang, X. Zheng, J. LiZ. Zha, Ginsenoside Rb1/TGF-β1 loaded biodegradable silk fibroin-gelatin porous scaffolds for inflammation inhibition and cartilage regeneration, Mater. Sci. Eng. C Mater. Biol. Appl. 111 (2020) 110757, https://doi.org/10.1016/j.msec.2020.110757.